Electronic Supplementary Information for

Uniform poly(phosphazene-triazine) porous microspheres for highly efficient iodine removal

Shaohui Xiong,[a] Jian Tao,[a] Yuanyuan Wang,[a] Juntao Tang,[a] Cheng Liu,[b] Qingquan Liu,[c] Yan Wang,[a] Guipeng Yu,*[a, b] and Chunyue Pan*[,a]

[a] *College of Chemistry and Chemical Engineering, Hunan Provincial Key Laboratory of Efficient and Clean Utilization of Manganese Resources, Central South University, Changsha 410083, China. E-mail: gilbertyu@csu.edu.cn, panchunyue@csu.edu.cn*

[b] *State Key Laboratory of Fine Chemicals, Dalian University of Technology, Dalian 116012, China.*

[c] *Institute of Materials Science and Engineering, Hunan University of Science and Technology, Xiangtan 411201, China*

Table of Contents

Section 1. Materials and Measurements

Materials

All chemical reagents and solvents were of analytical-grade and used as obtained without further purification unless stated otherwise. Hexachlorocyclotriphosphazene (HCCP), melamine, 4-aminobenzonitrile, trifluoromethanesulfonic acid and triethylamine (TEA) was produced by Energy Chemical Co., Ltd. Super dry dimethyl sulfoxide (DMSO, 99.7%) were purchasedfrom J&K scientific Co., Ltd.

Measurements

Fourier transform infrared (FT-IR) spectra

Fourier transform infrared (FT-IR) spectra were operated on a Thermo Nicolet Nexus 380 FT-IR instrument employing KBr pellets.

Magic-angle spinning solid-state ^{13}CNMR spectra

Magic-angle spinning solid-state ^{13}CNMR spectra were recorded on a Bruker Avance III 400 NMR spectrometer. The spectra were measured using a contact time of 2.0 ms and a relaxation delay of 10.0 s.

Thermogravimetric analysis (TGA)

Thermogravimetric analyses (TGA) were performed on a Mettler TGA/SDTA851 thermogravimetric analysis instrument under nitrogen flow with a heating rate of 10 ^{o}C/min rang from 0 to 750 ^{o}C.

UV-vis absorption spectra (UV-vis)

UV-vis absorption spectra were measured using a Hitachi U-5100 spectrophotometer.

Fluorescence spectroscopy

The solid-state fluorescence spectroscopes were recorded with a front surface accessory on a FLS920 fluorescence spectrometer.

Scanning electron microscopy (SEM)

Scanning electron microscopy was performed on a FEI SIRION200 microscope under scanning voltages of 10 kV. Before testing, gold granules was labeled with the samples.

Transmission electron microscopy (TEM) and Energy dispersive X-ray spectrometry (EDS)

High resolution TEM and EDS were carried out on a JEOL JEM-2100F microscope operating at an accelerating voltage of 200 kV and attached with a EDS spectrometer. Before measurement, the samples were dispersed in anhydrous ethanol in ultrasonical bath and dropped on a honey carbon film coated with a copper grid.

Powder X-ray diffraction (PXRD)

Wide-angle PXRD data were recorded using INEL CPS 120 powder diffractometer equipped with Ni-filtered Cu Kα radiation (40 kV, 100 mA) with 2θ ranging from 5° to 60°.

Nitrogen adsorption-desorption isotherm measurement

The dry state polymer surface areas and pore characteristics were conducted on a Micromeritics ASAP 2020 adsorption analyzer by nitrogen sorption at 77 K. Prior to each measurement, the samples were activated at 100 ^{o}C for 10 h under vacuum. About 100 mg of polymer was employed for each gas sorption measurement. The specific surface areas (SBET) were calculated using Brunauer-Emmett-Teller (BET)

model. The pore size distributions were derived from adsorption isotherms based on non-local density functional theory (NLDFT).

Element analysis (EA)

C, H, N content of the samples were determined by using a Vario ELIII CHNOS elemental analyzer.

Detailed operating steps for the capture of iodine vapor

The iodine vapor capture experiment was carried out according the following procedure. Two small weighing bottles were separately charged with activated MelPOP-2 (16.00 mg) and TatPOP-2 (16.00 mg). Then the bottles were placed in a sealed glass container equipped with excess iodine pellets at the bottom. The container was vacuumized and heated at 75 °C under ambient pressure. Thereafter, the samples were cooled down to room temperature and weighed at different time intervals. The iodine uptakes of samples were calculated by weight gain according to: $\alpha = [(m_2 - m_1)/m1] \times 100$ wt %, where α is the iodine uptake, m_1 and m_2 are the mass of POPNs before and after adsorption of iodine. The iodine capture experiments were repeated three times to ensure the data was authentic and dependable.

Detailed operating steps for the capture of iodine in organic solution

The iodine capture experiment in organic solution was carried out according the following procedure. To study the iodine uptake capacity of POPNs in organic solution, the activated samples with the same weight (16.00 mg) were immersed into iodine/n-hexane (8.00 mmoL/L). Then the supernatant (2.00 mL) was gauged by employing UV − vis at different time intervals.

Detailed experiment prodcues for the release of iodine in organic pahse

Iodine release came into being when the iodine-loaded samples (12.00 mg) were immersed in organic solvents such as ethanol (4.00 mL) at room temperature. The iodine release behavior was monitored by the UV−*vis* absorbance of the iodine-including ethanol within the monitored time frame.

Section 2. Synthesis and Characterization of TAPT, POPNs

4,4',4''-(1,3,5-triazine-2,4,6-triyl)trianiline:

At 0 ^{o}C, a 50-ml round-bottom flask was charged with 4-aminobenzonitrile (1.55 g, 13.00 mmol) under N_2 atmosphere, after 20min, then 4.00 mL of trifluoromethanesulfonic acid was added dropwise via a syringe. The mixture was stirred at 0 ^{o}C for 20 min. The mixture was then warmed to room temperature and stirred for additional 24 h. The resulting mixture was diluted with distilled water (20.00 mL), then washed with NaOH aqueous solution (2 M) until the washing water exhibited pH=7. The precipitate was collected by filtration after washing with distilled water for several times and dried under vacuum to obtain the targeted product (5.9 g, 79%) 1H NMR (400 MHz, DMSO-d6): 7.75-7.7(d, 6H), 6.68-6.64 (d, 6H), 5.97 (s, 6H).

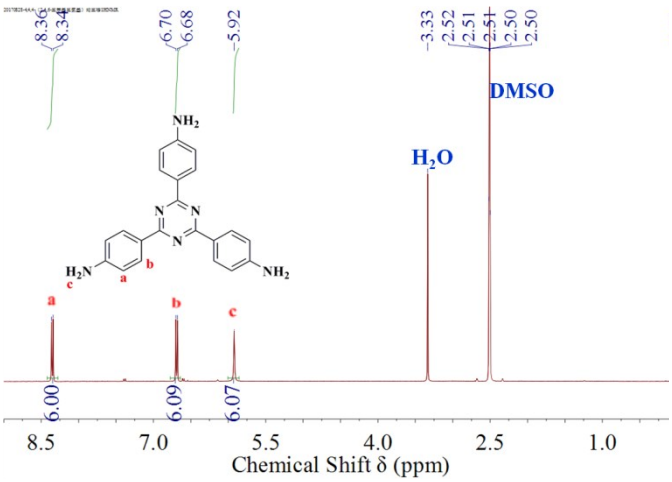

Fig.S0 ^{1}HNMR (400 MHz, DMSO-d_6) spectrum of TAPT

Preparation of MelPOP – 2. To a solution of HCCP (700 mg, 2.00 mmoL), melamine (508 mg, 4.00 mmoL), N,N-dimethylformamide (7 mL) and triethylamine (5 mL) was added in a glass ampoule under N_2 atmosphere. The mixture was concussed for 30 min and then degassed by three freeze-pump-thaw cycles. And then the tube was sealed under vacuum condition and warmed to room temperature. The mixture was heated up to 125 °C for 5 days. Cool down to room temperature, the precipitation was filtered off and successively washed with distilled water, tetrahydrofuran and dichloromethane for several times. The filter cake was soxhlet extracted with methanol, tetrahydrofuran and acetone for 24 h and dried under vacuum. The product was gained as pale white powder (MelPOP-2, yield: 90 %).

Preparation of TatPOP – 2 TatPOP–2 was prepared employing the same procedure originating from HCCP (700 mg, 2.00 mmol) with TAPT (1.43 g, 4.00 mmol) as for MelPOP-2. Likewise, triethylamine (7 mL) and N,N-dimethylformamide (7 mL) were used as acid-binding agent and solvent. There is no obvious difference in synthesis condition and aftertreatment procedures between TatPOP-2 and MelPOP-2. The polymers were gained as khaki powder (yield: 93%).

Fig. S1

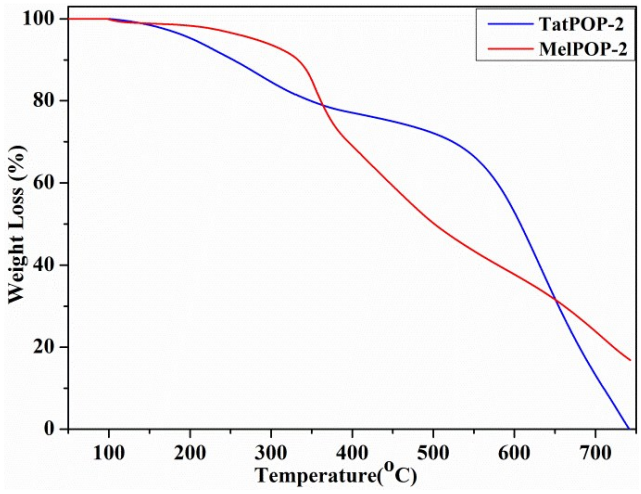

Fig. S1 TGA curves of POPNs.

Fig. S2

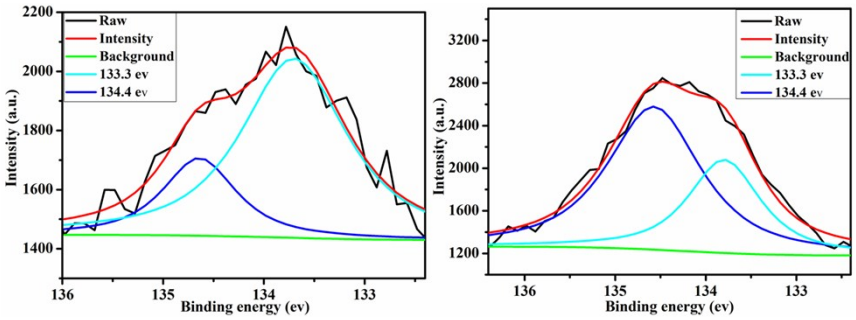

Fig.S2 XPS spectra of P spectra for MelPOP-2 and TatPOP-2 (left to right).

Fig. S3

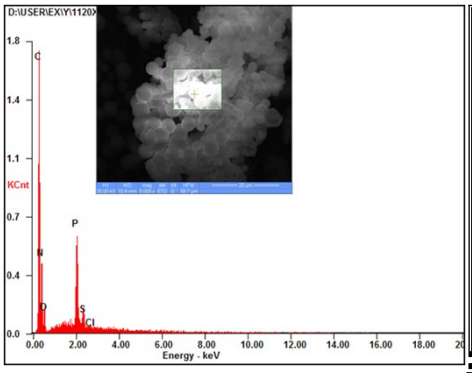

Element	Wt%	At%
CK	44.27	50.46
NK	39.84	38.95
OK	08.68	07.43
PK	05.89	02.60
SK	01.22	00.52
ClK	00.11	00.04
Matrix	Correction	ZAF

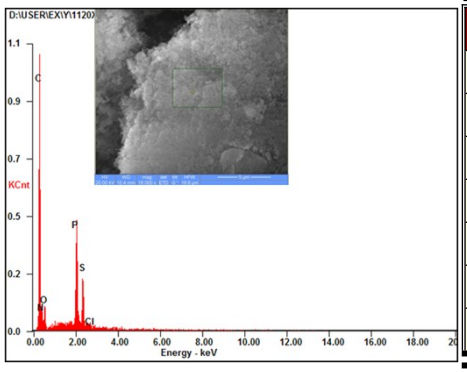

Element	Wt%	At%
CK	63.41	71.70
NK	15.89	15.40
OK	09.45	08.03
PK	07.07	03.10
SK	04.11	01.74
ClK	00.08	00.03
Matrix	Correction	ZAF

Fig. S3 The element content data of MelPOP-2 and TatPOP-2 (from up to down) by EDS analysis.

Fig. S4

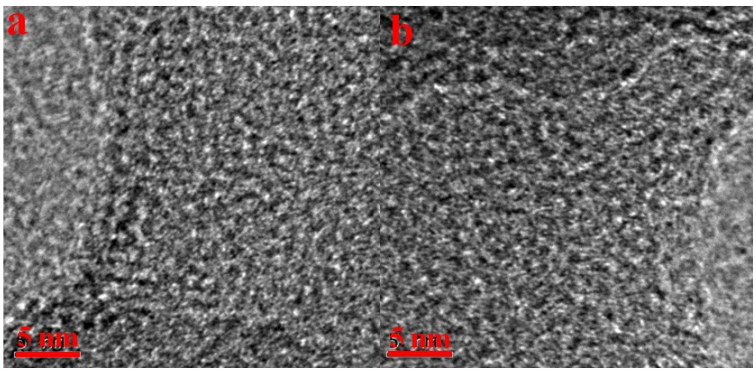

Fig. S4 The TEM images of a) **MelPOP-2**, b) **TatPOP-2**.

Fig. S5

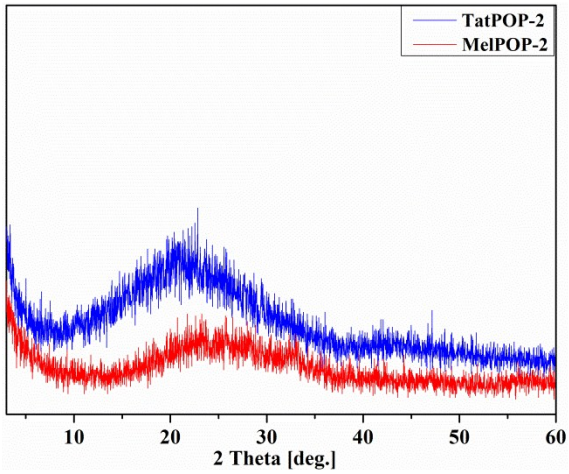

Fig. S5 Powder X-ray diffraction data for polymers

Fig. S6

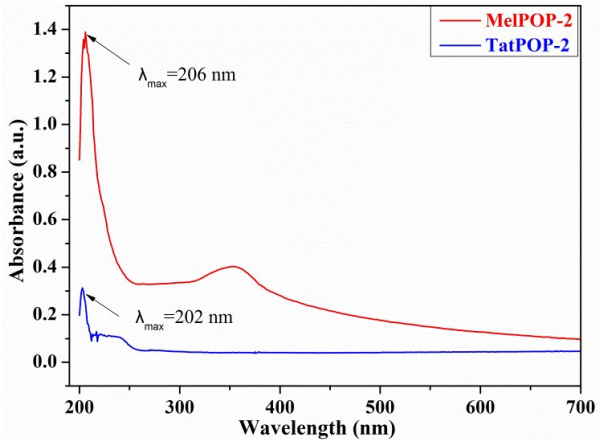

Solid UV-*vis* spectra of POPNs

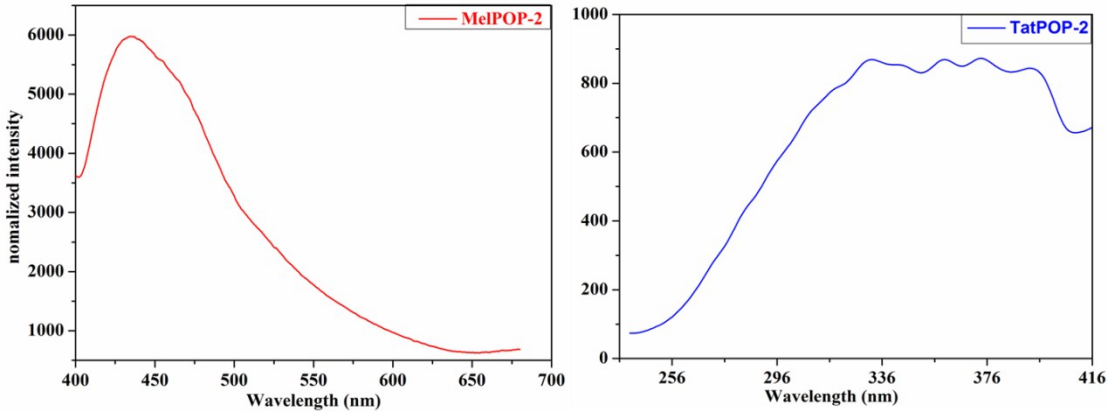

Fig. S6 Solid luminescent spectra of MelPOP-2 and TatPOP-2

Table S1 Pore parameters for polymers.

Sample	$SA_{BET}(m^2/g)$	$SA_{LAN}(m^2/g)$	$V_{Total}(cm^3/g)$
MelPOP-2	50.5	87.8	0.22
TatPOP-2	36.5	58.5	0.18

Fig. S7

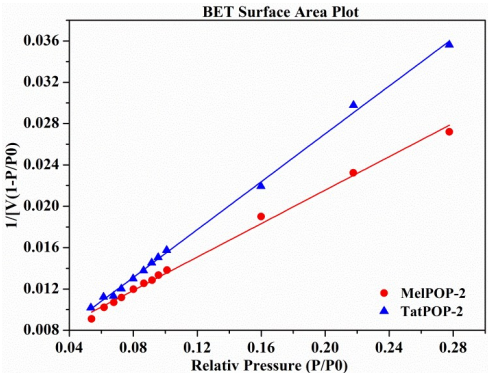

Fig. S7 BET surface area linear plot for POPNs.

Table S2 Summary of detailed iodine uptake properties for nanoporous organic materials.

Absorbent	T (°C)	Pressure	S_{BET} (m^2/g)	Ads I_2 per unit S_{BET} (wt/(m^2/g))	Ads I_2 (%)	References
TatPOP-2	75	1bar	50	9.00	450	This work
MelPOP-2	75	1bar	36	7.28	262	This work
BDP-CPP-1	75	1bar	635	0.45	283	Ref.1
HCMP-3	85	1bar	82	4.10	336	Ref.2
SCMP-2	77	1bar	855	0.26	222	Ref.3
SIOC-COF-7	75	1bar	618	0.78	481	Ref.4
AzoPPN	77	1bar	400	0.73	290	Ref.5
CMPN-3	70	1 bar	1368	0.15	208	Ref.6
PAF-24	75	1bar	136	2.03	276	Ref.7
PAF-23	75	1bar	82	3.30	271	Ref.7
PAF-25	75	1bar	262	0.99	260	Ref.7
Azo-Trip	77	1 bar	510	0.47	238	Ref.8
NiP-CMP	77	1 bar	2630	0.077	202	Ref.9
PAF-1	25	40 Pa	5600	0.033	186	Ref.10
NTP	75	1 bar	1067	0.17	180	Ref.11
JUC-Z2	25	40 Pa	2081	0.069	144	Ref.10
ZIF-8	75	1 bar	1875	0.064	120	Ref.12
Ag@Mon-POF	70	1 bar	690	0.036	25	Ref.13

References for Table S2

1. Yunlong Zhu, Ya-Jian Ji, De-Gao Wang, Yi Zhang, Hui Tang, Xin-Ru Jia, Min Song, Guipeng Yu and Gui-Chao Kuang. BODIPY-based conjugated porous polymers for highly efficient volatile iodine capture J. Mater. Chem. A, 2017,**5**, 6622-6629.

2. Y. Liao, J. Weber, B. M. Mills, Z. Ren and C. F. J. Faul, Highly efficient and reversible iodine capture in hexaphenylbenzene-based conjugated microporous polymers. Macromolecules, 2016, 49, 6322−6333.
3. X. Qian, Z. Zhu, H. Sun, F. Ren, P. Mu, W. Liang, L. Chen and A. Li, Capture and Reversible Storage of Volatile Iodine by Novel Conjugated Microporous Polymers Containing Thiophene Units. ACS Appl. Mater. Interfaces 2016, 8, 21063-21069.
4. Z.-J Yin, S-Q Xu, T-G Zhan, Q-Y Qi, Z-Q Wu and X Zhao, Ultrahigh volatile iodine uptake by hollow microspheres formed from a heteropore covalent organic framework. Chem. Commun., 2017, 53, 1-4.
5. H. Li, X. Ding and B.-H. Han, Porous azo-bridged porphyrin-phthalocyanine network with high iodine capture capability. Chem. Eur. J., 2016, 22, 11863 – 11868.
6. Y. Chen, H. Sun, R. Yang, T. Wang, C. Pei, Z. Xiang, Z. Zhu, W. Liang, A. Li, and W. Deng, Synthesis of conjugated microporous polymer nanotubes with large surface areas as absorbents for iodine and CO_2 uptake. J. Mater. Chem. A, 2015, 3, 87-91.
7. Z. Yan, Y. Yuan, Y. Tian, D. Zhang and G. Zhu, Highly efficient enrichment of volatile iodine by charged porous aromatic frameworks with three sorption sites. Angew. Chem. Int. Ed., 2015, 54, 12733−12737.
8. Q.-Q. Dang, X.-M. Wang, Y.-F. Zhan and X.-M. Zhang, An azo-linked porous triptycene network as an absorbent for CO_2 and iodine uptake. Polym. Chem., 2016, 7, 643−647.
9. S. A, Y. Zhang, Z. Li, H. Xia, M. Xue, X. Liu and Y. Mu, Highly efficient and reversible iodine capture using a metalloporphyrin-based conjugated microporous polymer. Chem. Commun., 2014, 50, 8495−8498.
10. C. Pei, T. Ben, S. Xu and S. Qiu, Ultrahigh iodine adsorption in porous organic frameworks. J. Mater. Chem. A, 2014, 2, 7179−7187.
11. H. Ma, J.-J. Chen, L. Tan, J.-H. Bu, Y. Zhu, B. Tan and C. Zhang, Nitrogen-rich triptycene-based porous polymer for gas storage and iodine enrichment. ACS Macro Lett., 2016, 5, 1039−1043.
12. D. F. Sava, T. J. Garino and T. M. Nenoff, Iodine confinement into metal−organic frameworks (MOFs): Low-temperature sintering glasses to form novel glass composite material (GCM) alternative waste forms. Ind. Eng. Chem. Res., 2012, 51, 614−620.
13. A. P. Katsoulidis, J. He and M. G. Kanatzidis, Functional monolithic polymeric organic framework aerogel as reducing and hosting media for Ag nanoparticles and application in capturing of iodine vapors. Chem. Mater., 2012, 24, 1937-1943.

Table S3 Element analysis of polymers

Sample	Element analysis (%)					
	Found			Anal. calcd		
	N	C	H	N	C	H
MelPOP-2	44.32	33.63	6.02	55.13	18.91	1.59
TatPOP-2	15.15	56.41	6.25	25.08	60.22	3.61

Fig. S8

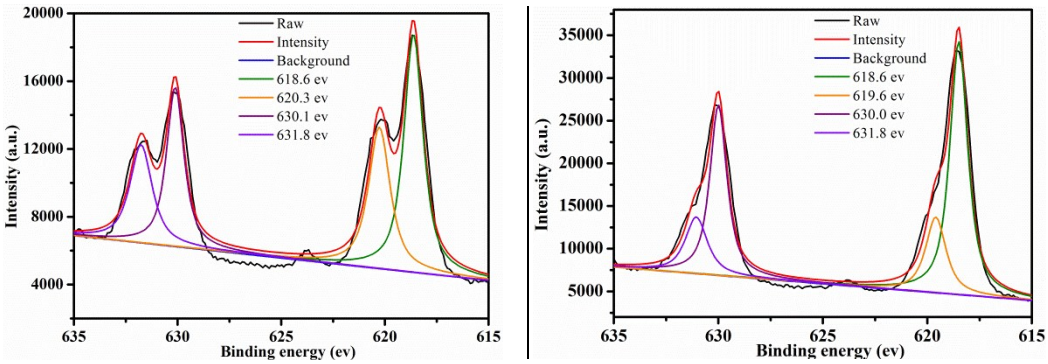

Fig. S8 XPS spectra of TatPOP-2@I_2 and MelPOP-2@I_2 (left to right).

Fig. S9

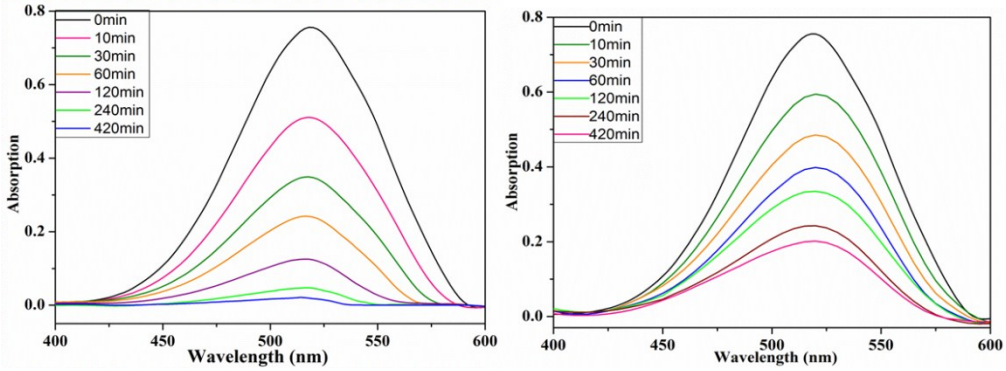

Fig. S9 UV-*vis* spectra for TatPOP-2 (16 mg, left) and MelPOP-2 (16 mg, right) in iodine-hexane solution (2mL, 8 mM) at various times.

Fig. S10

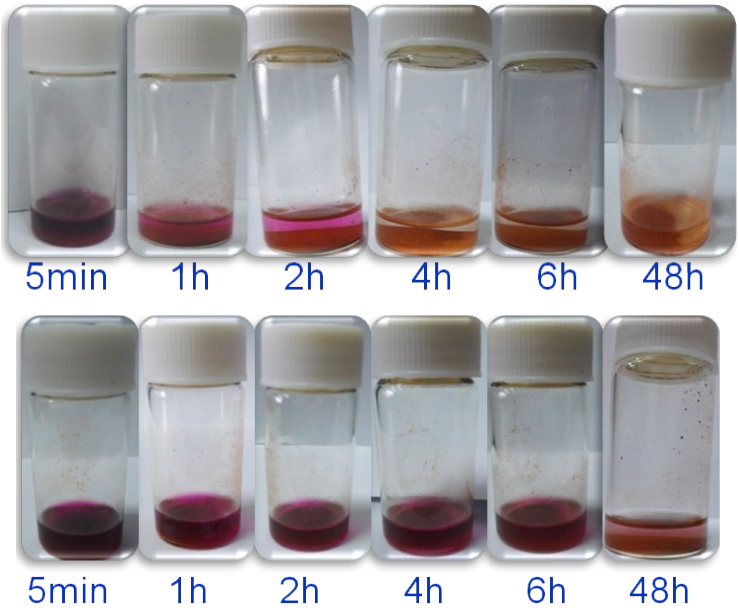

Fig. S10 Photographs showing progress of iodine capture after TatPOP-2 and MelPOP-2 (up to bottom) (16 mg) was immersed in a hexane solution of iodine (8.0 mmol/L, 2 mL).

Fig. S11

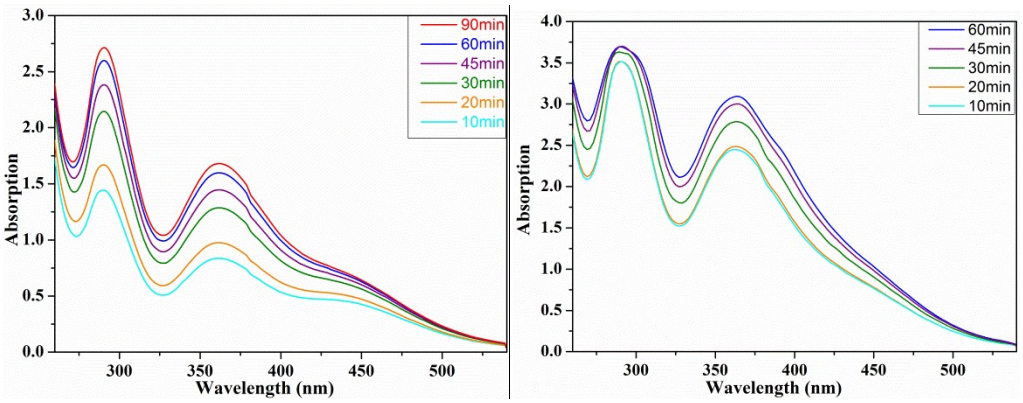

Fig. S11 UV-*vis* spectra of iodine released from MelPOP-2@I_2 (left) and TatPOP-2@I_2 (right) (12 mg) in 4 mL anhydrous ethanol.

Fig. S12

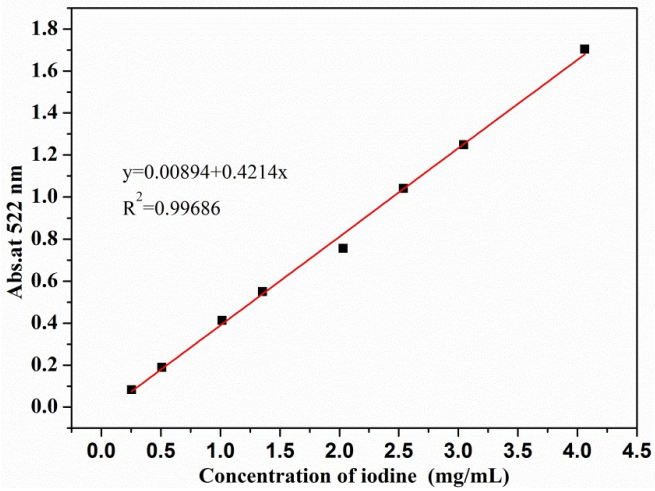

Fig. S12 Working curve for the estimation of iodine uptake in solution.

Fig. S13

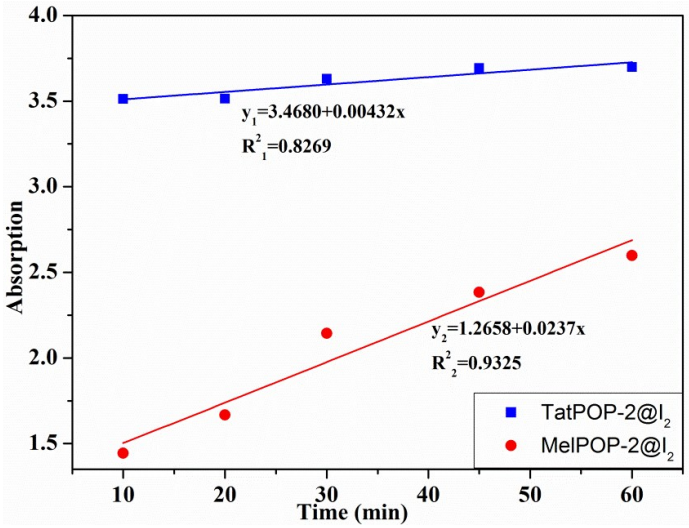

Fig. S13 The release rate of MelPOP-2@I_2 and TatPOP-2@I_2 in ethanol.